How to cite: *Angew. Chem. Int. Ed.* **2021**, *60*, 21033–21039
International Edition: doi.org/10.1002/anie.202108658
German Edition: doi.org/10.1002/ange.202108658

Nanomedicine

Exquisite Vesicular Nanomedicine by Paclitaxel Mediated Co-assembly with Camptothecin Prodrug

Zijian Zhou, Chao Du, Qianyu Zhang, Guocan Yu, Fuwu Zhang,* and Xiaoyuan Chen**

Abstract: *We report that the self-assembly of drug amphiphiles, Evans blue conjugated camptothecin prodrug (EB-CPT), can be modulated by another anticancer drug paclitaxel (PTX), resulting in ultrahigh quality of nanovesicles (NVs) with uniform shape and diameters of around 80 nm with the EB-CPT:PTX weight ratio of 1:1, 1:2, and 1:3, denoted as ECX NVs. Significantly, the co-assembly of EB-CPT and PTX without adding other excipients has nearly 100 % drug loading efficiency (DLE) and ultrahigh drug loading content (DLC) of PTX alone of up to 72.3 ± 1.7 wt % which, to our best knowledge, is among the highest level reported in literature. Moreover, the ECX NVs with the EB-CPT:PTX weight ratio of 1:2 showed remarkable combination index of 0.59 at a level of 50 % efficacy against HCT116 cells in vitro and greatly improved tumor inhibition effect in vivo compared with two clinically approved CPT- and PTX-based anticancer nanomedicines (Onivyde and Abraxane) individually and their combinations.*

Introduction

Self-assembly is one of the most interesting, if not the most important, processes that drive the evolution of biological architecture and functions in nature.[1] Over the past decades, the tremendous development of nanomedicine also underlies the essential role of self-assembly in tailoring a diverse population of nanomaterials for biomedical applications.[2] Owing to the presence of biological barriers, small-molecule-based therapeutic drugs may suffer from the poor solubility and suboptimal pharmacodynamics and pharmacokinetics in vivo, leading to poor drug delivery and utilization efficiency in the target-of-interest.[3] This is where nanomedicine comes in that nanomaterials loaded with therapeutic drugs are prone to be optimized on different parameters to meet the criteria for improved therapeutic outcomes.[4] Among various nanoparticle configurations (e.g., micelles, fibers), liposomes with vesicular structure have achieved the most success in clinical translation, including a recently approved siRNA nanomedicine by the US Food and Drug Administration (i.e., Onpattro).[5] Although reasons to the success are not clearly understood, the mimetic architecture of liposomal nanoparticles to cell membrane structure may play an important part.[6] To this end, there has been a great deal of effort to explore liposome-like vesicular structures as delivery vehicles in nanomedicine.[7]

Molecular agents can be incorporated with nanoparticles through different driving forces, such as van der Waals adsorption and chemical conjugation.[8] For lipid nanoparticles, both hydrophilic and hydrophobic molecules could be loaded in the inner space and on the membrane of vesicles, respectively.[9] To facilitate the self-assembly, however, most liposomal vesicles have a typically low drug loading content (DLC), around or less than 10 % in weight (wt). For polymer-based drug conjugates, the DLC is often even lower due to the relatively large contribution of weight from the polymer scaffolds.[6b] As a result, a large portion of these excipients in nanomedicine may impose extra burden to patients and cause systemic toxicity when high doses are acquired.[10] Therefore, the research interest in pursuing high drug loading nanomedicine with minimal excipients has gained great momentum, especially for liposomes and liposome-like vesicular nanomedicine.[11] For example, Shen et al. used oligomer ethylene glycol conjugated anticancer drug camptothecin (CPT) to mimic phospholipid structure and assembled nanocapsules, resulting in a high DLC of CPT up to 58 wt %.[12] Liang et al. prepared a CPT-floxuridine conjugate amphiphile

[*] Dr. Z. Zhou, C. Du, Q. Zhang
State Key Laboratory of Molecular Vaccinology and Molecular Diagnostics, Center for Molecular Imaging and Translational Medicine, School of Public Health, Xiamen University
Xiamen 361102 (P. R. China)
E-mail: zhouz@xmu.edu.cn
Dr. G. Yu
Key Lab of Organic Optoelectronics & Molecular Engineering, Department of Chemistry, Tsinghua University
Beijing 100084 (P. R. China)
Dr. F. Zhang
Department of Chemistry, University of Miami
Miami, FL 33146 (USA)
E-mail: fxz174@miami.edu
Prof. X. Chen
Departments of Diagnostic Radiology, Chemical and Biomolecular Engineering, and Biomedical Engineering, Yong Loo Lin School of Medicine and Faculty of Engineering
National University of Singapore
Singapore 117597 (Singapore)
and
Clinical Imaging Research Centre, Centre for Translational Medicine, Yong Loo Lin School of Medicine, National University of Singapore
Singapore 117599 (Singapore)
and
Nanomedicine Translational Research Program, NUS Center for Nanomedicine, Yong Loo Lin School of Medicine
National University of Singapore
Singapore 117597 (Singapore)
E-mail: chen.shawn@nus.edu.sg
Supporting information and the ORCID identification number(s) for the author(s) of this article can be found under: https://doi.org/10.1002/anie.202108658.

that itself could self-assemble into liposomal nanomedicine with considerably high DLC.[13] More recently, paclitaxel (PTX), one of the most widely used anticancer drugs, was reported to promote the self-assembly of PTX-based amphiphiles, Spheropax, from micelles to filament structures.[14] Hence, we speculated that PTX may serve as a mediator to promote the co-assembly with other amphiphiles, which could therefore attain nanomedicine with enhanced DLC. Considering the efficient activity of PTX and the potential synergistic effect in combination therapy,[15] the success to this hypothesis may provide important insight into translational nanomedicine.[7,16] Clinical trials on the combination therapy of PTX and CPT have been studied in non-small-cell lung cancer, showing appreciable activity and favorable survival data.[17] However, the combination study on different cell lines was reported with controversial results using the sequential dosing regimen, which aroused great interest to optimize the model for PTX and CPT combination therapy.

Here, we report an interesting work on PTX mediated co-assembly with an amphiphilic prodrug, Evans blue conjugated CPT molecules (EB-CPT). Previously, we have shown that EB-CPT could spontaneously self-assemble into micelle-like particles, attaining transformative behavior in vivo and effective anticancer activity.[8] In the current work, we first optimized the synthetic route of EB-CPT to facilitate the scale-up production and further potentiate the clinical translation. We then studied the effect of PTX in mediating the self-assembly of EB-CPT by tuning the weight ratios between them. The obtained nanomedicine by co-assembly of EB-CPT and PTX with different weight ratios were further evaluated on the anticancer efficiency both in vitro and in vivo. This work may provide important insight into the strategy of orchestrating combination therapy through nanomedicine.[15,18]

Results and Discussion

This work started from optimizing the chemistry for synthesizing EB-CPT, where an alkyl primary amine, rather than an aromatic primary amine, was used in the conjugation step, to attain significantly higher reaction efficiency, less side reactions, and easier purification with a high yield (Scheme S1 and Figure S1–S5). The new EB-CPT has a carbamate linker rather than an ester linker compared with our previously reported EB-CPT structure, while the major chemistry (e.g., GSH responsive CPT release) was identical. The amphiphilic property of EB-CPT led to the self-assembly into particles

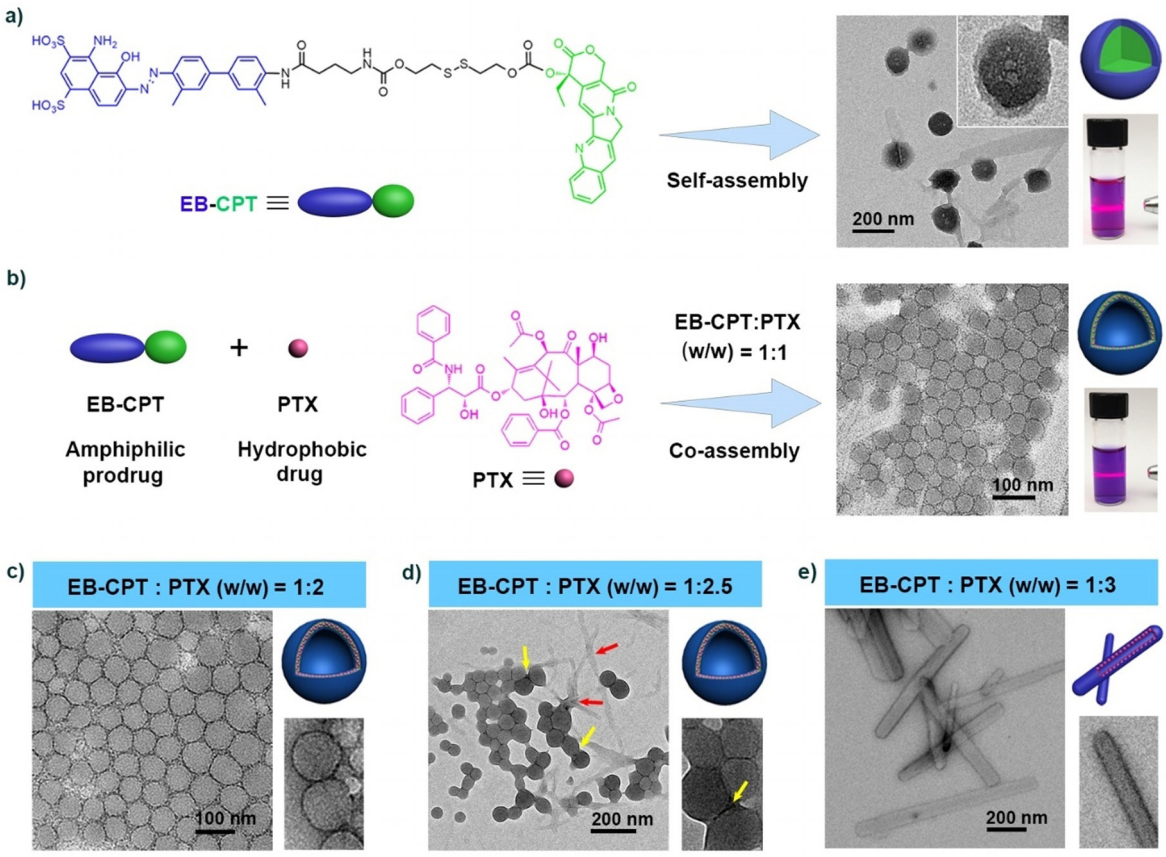

Figure 1. a) Illustration of the self-assembly of EB-CPT alone and the obtained TEM image of the EB-CPT particles. b) Illustration of the co-assembly of EB-CPT and PTX with weight ratio (w/w) of 1:1, and the obtained TEM image of ECX NVs. The cartoon of respective nanoparticles and the photo of nanoparticle solution shone with a laser pen are shown on the right. c)–e) TEM images of the ECX NVs with different weight ratios, 1:2, 1:2.5 and 1:3, respectively. Red arrows indicate the fiber-like structure and yellow arrows indicate the fusion structure of vesicles. The respective cartoons and the zoomed-in TEM images are shown on the right.

when directly dissolved in deionized water (Figure 1a). From the transmission electron microscopy (TEM) image, the EB-CPT particles have relatively uniform size with diameters of around 110–130 nm. The images showed that the EB-CPT particles were not compact architecture but with vacuoles inside the structure (Figure 1a, inset), indicating the domain formation during the self-assembly process. Although the self-assembly mechanism remains to be elucidated, this observation partially explains the formation of particles with such large diameters greatly exceeding the size of EB-CPT molecules. We then performed the co-assembly study of EB-CPT with PTX using a typical solvent-evaporation method. In our optimized procedure, 40 μL of EB-CPT (5.0 mg mL^{-1}) and 40 μL of PTX (5.0 mg mL^{-1}) in methanol were mixed and added dropwise into 2 mL of deionized water (Figure S6). After the removal of organic solvent in a ventilating fume hood, the obtained solution was clear without any observable precipitation, indicating the successful co-assembly of EB-CPT and PTX. Unexpectedly, we found that the co-assembly of EB-CPT and PTX with weight ratio (w/w) of 1:1 (molar ratio is 1:1.35) led to the formation of nanovesicles, denoted as ECX NVs hereafter. The ECX (1:1) NVs showed uniform vesicular shape with well-ordered self-assembly pattern on the TEM grid (Figure 1b and Figure S7a). The averaged diameter of ECX (1:1) NVs is 81.4 nm with a narrow size deviation ($\sigma = 4.1$) from the TEM images, which is also consistent with the hydrodynamic diameter of 96.4 ± 17.6 nm according to the dynamic light scattering (DLS) measurements (Figure S7b). The vesicular architecture of the ECX NVs was further characterized by voltage-adjusted TEM and cryoEM measurements (Figure S8). The slightly smaller size of ECX (1:1) NVs compared with that of EB-CPT particles was also revealed from the Tyndall light scattering patterns of both solutions (Figure 1a&b, lower right). Moreover, the ECX (1:1) NVs solution showed a blue color which was slightly different from the purple-red color of the EB-CPT particles solution. This was also observed from the absorption spectrum for the ECX (1:1) NVs and the EB-CPT particles which were 568 and 560 nm, respectively (Figure S9). This phenomenon implies the existence of weak intermolecular interactions between EB-CPT and PTX, which could mediate the co-assembly process.[19]

Encouraged by those results, we further explored the effect of w/w ratio of EB-CPT and PTX to the co-assembly behavior. Under the same condition, however, the w/w ratio of EB-CPT:PTX of 1:0.5 led to the formation of ECX nanoparticles with diameters close to that of EB-CPT particles, but with prominent amorphous structure similar to that observed from EB-CPT alone nanoparticles (Figure S10). We further found that increasing the w/w ratio of EB-CPT:PTX to 1:2 also led to the formation of uniform ECX NVs (Figure 1c and Figure S11). By tracking the self-assembly process of the ECX NVs, we observed the formation of precursor structures at the early time points which transformed into vesicular structures with the evaporation of organic solvents (Figure S12). The size of ECX NVs increased to around 130 nm with the EB-CPT:PTX ratio (w/w) of 1:2.5 (Figure 1d). Moreover, the fiber-like structure (red arrow) and vesicular fusion (yellow arrow) were observed in the TEM of ECX (1:2.5) NVs. Interestingly, further increasing this ratio to 1:3 under the same conditions obtained tube-like vesicular structures with width of about 70 nm and length of about 1 micrometer (Figure 1e). Therefore, the amount of added PTX may alter the kinetics of the formation of hydrogen bond network among hydrophobic units, which directs the molecular rearrangement and the growth of precursor structures into different morphologies. Unfortunately, significant precipitation was found when further increasing the w/w ratio to 1:4 for EB-CPT:PTX.

Noteworthy, the DLC of PTX in the ECX (1:2) NVs is 65.7 ± 0.5 wt % which, to the best of our knowledge, is among the highest values reported in the literature for PTX-based nanomedicine (Table 1 and Table S1). Moreover, another component of the ECX (1:2) NVs, EB-CPT, is also responsible for glutathione activated release of CPT, which turns into an additional 10.1 wt % DLC for CPT. The drug loading efficiency (DLE) of PTX characterized by high-performance liquid chromatography analysis was 99.6 ± 0.2 %, 99.4 ± 0.2 %, 99.1 ± 0.4 % and 97.3 ± 1.1 % for the w/w of EB-CPT:PTX of 1:1, 1:2, 1:2.5 and 1:3, respectively. It is noteworthy that the obtained ECX NVs solution could attain an ultrahigh concentration of PTX up to 0.3 mg mL^{-1} in water, which is over 600-fold higher than that of PTX alone (< 0.5 μg mL^{-1}).[20] Considering the merits of free of chemical conjugation in the ECX NVs which otherwise may greatly sacrifice the drug potency of PTX, the ECX NVs are promising platforms for PTX delivery and in cancer therapy.

Table 1: The drug loading content (DLC) and drug loading efficiency (DLE) of ECX nanomedicine with different w/w ratios of EB-CPT and PTX.[a]

Nanomedicine (EB-CPT:PTX)	DLC (CPT) [%]	DLC (PTX) [%]	DLE (CPT) [%]	DLE (PTX) [%]
ECX (1:1)	15.2	49.1 ± 0.7	100	99.6 ± 0.2
ECX (1:2)	10.1	65.7 ± 0.5	100	99.4 ± 0.2
ECX (1:2.5)	8.67	70.1 ± 0.8	100	99.1 ± 0.4
ECX (1:3)	7.58	72.3 ± 1.7	100	97.3 ± 1.1

[a] DLE of 100 % for CPT indicated no measurable residual EB-CPT during the co-assembly. Data are presented as mean ± s.d.

The critical aggregation concentration (CAC) of amphiphile-based nanomedicine is an important factor for drug delivery systems.[21] To explore the colloidal stability of ECX NVs in solution, we studied the behavior of particle formation by diluting the existing ECX NVs. We first practiced the ECX (1:2 w/w) NVs and found that dilution could mediate the change of shape from original nanovesicles (at a concentration of 100 and 200 μg mL^{-1} of EB-CPT and PTX, respectively) to fused vesicular structures with enlarged size (8 and 4 μg mL^{-1} for EB-CPT) (Figure 2a,b). Interestingly, at an extremely low concentration of 0.4 μg mL^{-1} of EB-CPT, we still observed nanoparticles from the TEM images albeit of size divergence. It is remarkable that the nanoparticle solution remained well-dispersible without any precipitation by dilution, indicating that PTX molecules were still loaded in the nanoparticles. Similar experiments were also performed on ECX (1:3 w/w) tube-like vesicles (Figure 2c,d). The results showed that

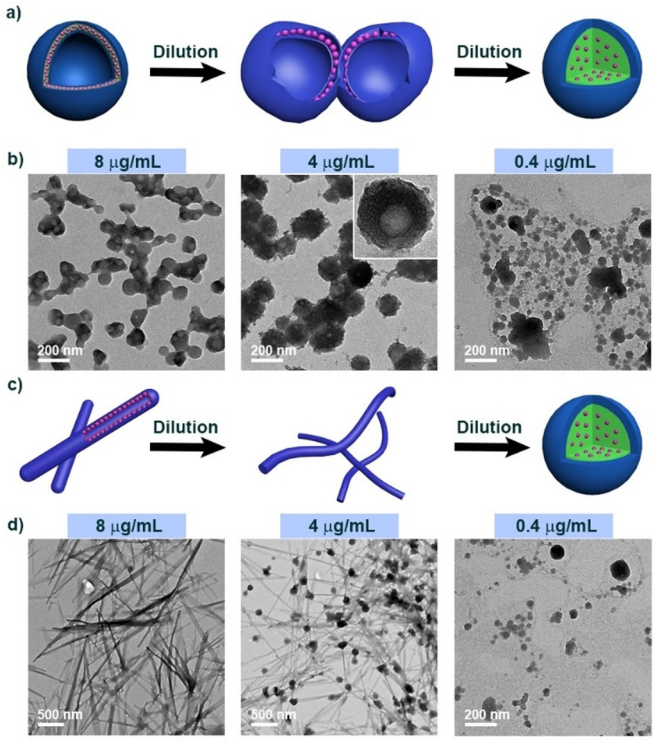

Figure 2. a),b) Illustration and TEM images of ECX 1:2 w/w NVs at different concentrations of EB-CPT. Dilution from 8 $\mu g\,mL^{-1}$ to 4 and 0.4 $\mu g\,mL^{-1}$ (for EB-CPT) led to the fusion of vesicles and the formation of particles. c, d) Illustration and TEM images of ECX 1:3 tube-like NVs at different concentrations of EB-CPT. Dilution from 8 $\mu g\,mL^{-1}$ to 4 and 0.4 $\mu g\,mL^{-1}$ (for EB-CPT) led to the transformation from tube-like structures to fibers and particles.

dilution could transform the original tube-like vesicles (at a concentration of 100 and 300 $\mu g\,mL^{-1}$ of EB-CPT and PTX, respectively) to fibers and particles at low concentrations. The calculated CAC of EB-CPT alone is 1.5 $\mu g\,mL^{-1}$ in aqueous solution. Although the shape changed from vesicles to particles, the presence of PTX greatly improved the colloidal stability of EB-CPT especially for the concentrations below the CAC value, which further implies the intermolecular interactions between EB-CPT and PTX molecules. Furthermore, these results indicate that the vesicular shape is most likely derived from a meticulous cooperation between hydrophobic interactions, intermolecular interactions and shearing force in the solution, etc.[6b]

To explore the anticancer potential of the ECX nanomedicine, we systematically evaluated the cytotoxicity of different components in vitro in three cancer cell models, HCT116, BxPC3, and U87MG. We first used MTT (3-(4,5-dimethylthiazol-2-yl)-2,5-diphenyltetrazolium bromide) assay to study the cell survival profiles of EB-CPT, CPT, Onivyde, PTX and Abraxane in HCT116 cells after 48 h incubation (Figure 3a). The obtained IC_{50} values were 0.3795, 0.087, 49.28, 0.01165 and 0.009455 μM for EB-CPT, CPT, Onivyde, PTX and Abraxane, respectively. We then studied the cytotoxicity of both ECX nanomedicine (nano combo) with different w/w ratios and the corresponding mixture combinations (mix combo). Due to the 30-fold difference in anticancer potency between EB-CPT and PTX, we hereafter refer to the PTX concentration to compare the IC_{50} values between different groups. Form the cytotoxicity profiles of the mix combo groups on HCT116 cells, the IC_{50} values of PTX had a significant drop from high to low w/w ratios for EB-CPT:PTX, i.e., 0.06086, 0.0981, 0.001588, 0.004522 and 0.002922 μM for w/w ratios of 1:0.5, 1:1, 1:2, 1:2.5 and 1:3 samples, respectively (Figure 3b). The IC_{50} values obtained from the cytotoxicity profiles of the nano combo groups to HCT 116 cells were 0.1509, 0.007749, 0.006638, 0.008919 and 0.0056 μM for the w/w ratios of 1:0.5, 1:1, 1:2, 1:2.5 and 1:3 ECX samples, respectively (Figure 3c).

We further studied the combination index (CI) of both mix combos of EB-CPT and PTX and ECX nano combos at the level of 50% efficacy against HCT116 cells (Figure 3d and Figure S13). The CI values of mix combos varied from 6.26, 9.25, 0.14, 0.41, to 0.26 for the w/w ratio of EB-CPT:PTX of 1:0.5, 1:1, 1:2, 1:2.5 and 1:3, respectively. In contrast, the CI values of the ECX nano combos are 1.55, 0.73, 0.59, 0.79, and 0.5 for the w/w ratio of 1:0.5, 1:1, 1:2, 1:2.5 and 1:3, respectively. The overall favorable CI values for the nano combo groups compared with those of mix combo groups could be due to the varied cellular uptake efficiency and the delivery kinetics of free drug components for EB-CPT and PTX. Interestingly, the combination of EB-CPT and PTX at a higher PTX content (w/w ratio of 1:1, 1:2, 1:2.5, and 1:3) showed mainly synergistic ($CI < 1$) effect, in sharp contrast to antagonistic ($CI > 1$) effect for the low PTX content (w/w ratio of 1:0.5) for both mix combo and nano combo samples. The mechanism of action for the synergy between CPT and PTX was studied with G2/M phase cell cycle arrest and changes in microtubule dynamics.[22] The dramatic different CI values for the w/w ratio of 1:1 for both mix combo (9.25) and nano combo (0.73) samples indicate that the formation of nanomedicine may serve as an efficient way to modulate the cellular uptake behavior especially for combination therapy. These results further underscore a vantage point of combination nanomedicine which endows an efficient platform integrating multiple components with controllable physiological and biological effects for facilitated clinical translation. Under the same conditions, the cytotoxicity studies were further evaluated on BxPC3 and U87MG cell lines (Figure S14 and S15). The IC_{50} values of free EB-CPT, CPT, Onivyde, PTX and Abraxane against BxPC3 and U87MG cells were similar to those on HC116 cells (Table S2). However, we found it interesting that both BxPC3 and U87MG cells were less sensitive to the cell killing effect for both mix combo and nano combo samples than HCT116 cells. For example, the IC_{50} value for ECX 1:2 w/w NVs is 0.006638 μM to HCT116 cells which is two-fold and 10-fold lower than that to BxPC3 and U87MG cells, 0.01029 and 0.1265 μM, respectively (Table S3). As a result, both mix combo and ECX nano combo samples at different w/w ratios showed antagonistic effect ($CI > 1$) to both BxPC3 and U87MG cells (Figure 3e,f and Figure S16).

Encouraged by the cell cytotoxicity results in vitro, we further conducted the antitumor study on a HCT116 xenograft tumor model. We chose ECX 1:2 w/w NVs to study the anticancer effect in vivo due to the excellent synergy in vitro

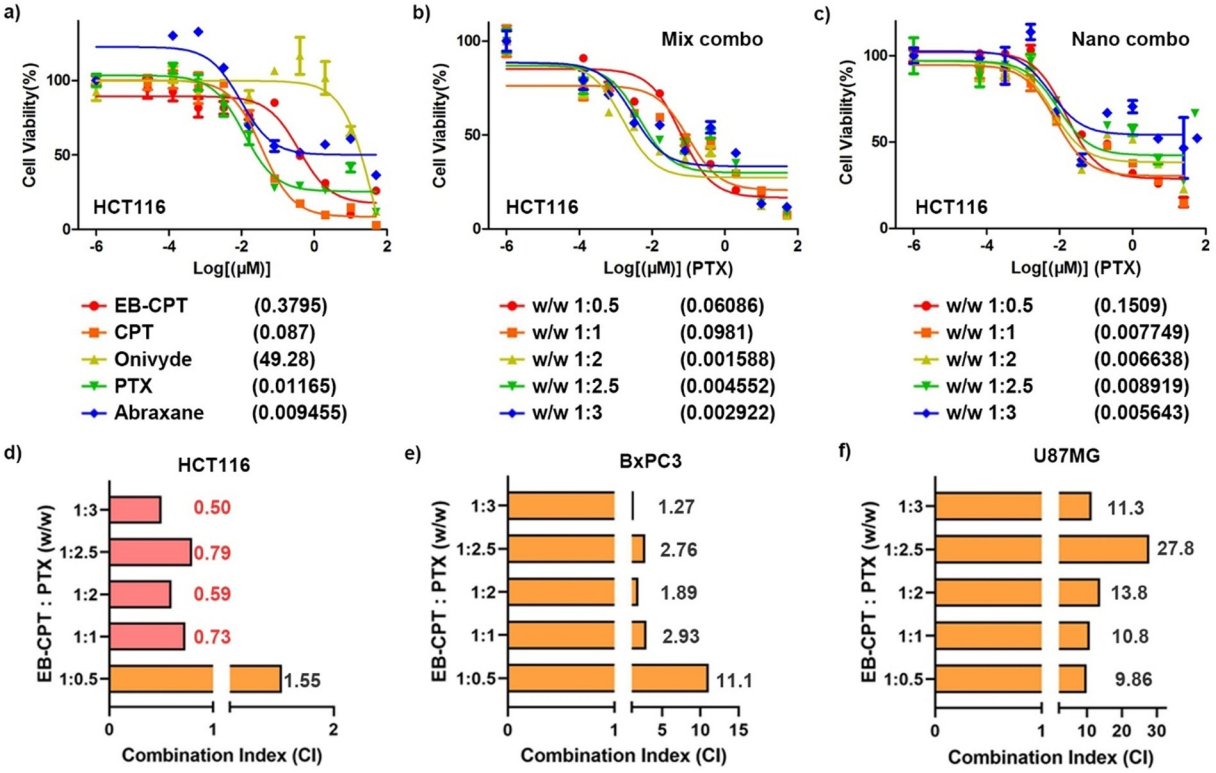

Figure 3. a) Cytotoxicity profiles of EB-CPT, CPT, Onivyde, PTX, and Abraxane against HCT116 cells in vitro by MTT assay. b),c) Cytotoxicity profiles of EB-CPT and PTX combinations against HCT116 cells, mix combo (b) and ECX nano combo (c) of EB-CPT and PTX with different weight ratios. d)–f) Columns show the CI at the 50% efficacy of ECX nanomedicine with different w/w ratios against HCT116, BxPC3, and U87MG cells, respectively. Pink and yellow color bars represent for synergistic (CI < 1) and antagonistic (CI > 1) effect, respectively.

and the biologically favorable size when comparing to that of ECX 1:3 w/w tube-like structure. Six randomly organized mouse groups ($n = 5$/group) with averaged tumor sizes of around 40–45 mm^3 were treated with saline, Onivyde (O), Abraxane (A), O + A (1:2 w/w), free mix combo (EB-CPT:PTX = 1:2 w/w), and ECX 1:2 w/w NVs, respectively. Each mouse group was treated with five doses every three days from day 0 to day 12. Each dose represented 1 $mg\,kg^{-1}$ of EB-CPT and 2 $mg\,kg^{-1}$ PTX or equivalently 3 $mg\,kg^{-1}$ drug compositions to the mouse body weight.

The mouse group treated with free mix combo drugs (EB-CPT plus PTX at a ratio of 1:2 w/w) had a significant drop in the mouse body weight due to the unavoidable systemic toxicity of free drug components (Figure 4a, star pink). This mouse group was then sacrificed at the day 12 due to the euthanasia criteria of over 20% drop of body weight. In contrast, the mouse groups treated with nanomedicine components showed relatively small changes in the body weight, potentiating the generally low side toxicity of nanomedicine. As a result, the mouse group treated with ECX 1:2 w/w NVs showed a significantly improved survival rate under an observation period of 46 days (Figure 4b). On the other hand, even though the mouse groups treated with Onivyde, Abraxane, and O + A (1:2 w/w) showed much improved late-time survival rate, the tumor inhibition rate (21.4%, 42.6%, and 48.8%, respectively) at the day 18 was not satisfactory (Figure 4c). Moreover, the slightly improved tumor inhibition rate for the O + A (1:2 w/w) group compared with the

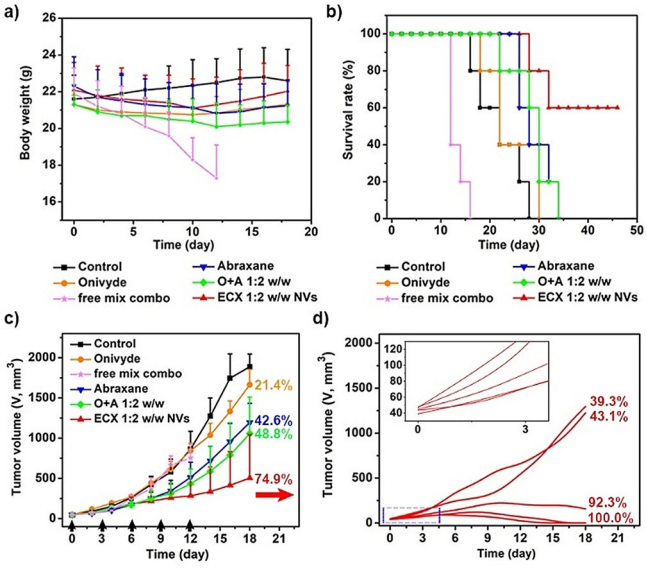

Figure 4. The antitumor study of the ECX NVs. a),b) Changes of mouse body weight and survival rate of mouse groups treated with different components. Data shown as mean ± s.d. c) The tumor volume change curves of mouse groups treated with different components. The mouse groups were treated with different components for five doses every three days from day 0 (black arrows). The percentage numbers after each curve indicates the tumor inhibition rate compared to the control group. Data shown as mean ± s.d. d) The individual tumor growth curves and the respective tumor inhibition rates of mouse groups treated with ECX 1:2 w/w NVs.

individual Onivyde and Abraxane groups indicates the negligible synergistic effect between Onivyde and Abraxane in vivo in our model. This corroborates with the results derived from in vitro cell cytotoxicity studies, which could be due to the spatiotemporally nonsynchronous biodistribution of the two individual drugs in vivo. Interestingly, the mouse group treated with ECX 1:2 w/w NVs showed remarkable tumor inhibition rate of 74.9%, in which two of the five mice had 100% tumor eradication at the day 18 and remained tumor-free for at least 46 days (Figure 4d and Figure S17). The hematoxylin-eosin (H&E) staining results of mouse major organs receiving different treatments further confirmed the unobvious toxicity of ECX NVs under the treatment regime (Figure S18). Taken together, the greatly improved tumor inhibition efficiency and favorably low side toxicity of the ECX NVs in vivo could be due to the unique mechanism of integrating CPT and PTX anticancer drugs.

Conclusion

We have shown that anticancer drug molecule PTX could mediate the self-assembly of another anticancer prodrug EB-CPT amphiphile with the shape changed from spherical particles to spherical vesicles and vesicular tube-like structures by tuning the weight ratios between EB-CPT and PTX. More importantly, the co-assembly of EB-CPT and PTX without other excipients has nearly 100% DLE and ultrahigh DLC of PTX, in addition to the uniform size and morphology. The obtained ECX NVs showed excellent synergistic anticancer effect against HCT116 cells in vitro. The antitumor study further demonstrated that ECX 1:2 w/w NVs are promising nanomedicine with spatiotemporally facilitated synergy between two anticancer drugs CPT and PTX and minimal side toxicity in vivo. This work provides an exquisite example of combining two anticancer drugs/prodrugs into vesicular nanomedicine through co-assembly strategy, which may open up new avenues and provide important insight into translational nanomedicine.

Acknowledgements

This work was supported by the Start-up fund from the Xiamen University (X2123305), the National University of Singapore Start-up Grant (NUHSRO/2020/133/Startup/08) and NUS School of Medicine Nanomedicine Translational Research Programme (NUHSRO/2021/034/TRP/09/Nanomedicine).

Conflict of Interest

The authors declare no conflict of interest.

Keywords: combination therapy · nanomedicine · nanovesicles · paclitaxel delivery · self-assembly

[1] a) G. M. Whitesides, B. Grzybowski, *Science* **2002**, *295*, 2418 – 2421; b) K. Das, L. Gabrielli, L. J. Prins, *Angew. Chem. Int. Ed.* **2021**, *60*, https://doi.org/10.1002/anie.202100274; *Angew. Chem.* **2021**, *133*, https://doi.org/10.1002/anie.202100274.

[2] a) H. Cui, M. J. Webber, S. I. Stupp, *Biopolymers* **2010**, *94*, 1 – 18; b) M. J. Webber, E. A. Appel, E. W. Meijer, R. Langer, *Nat. Mater.* **2016**, *15*, 13 – 26; c) G. Yu, B. Zhu, L. Shao, J. Zhou, M. L. Saha, B. Shi, Z. Zhang, T. Hong, S. Li, X. Chen, P. J. Stang, *Proc. Natl. Acad. Sci. USA* **2019**, *116*, 6618 – 6623; d) H. Duan, D. Wang, D. G. Kurth, H. Möhwald, *Angew. Chem. Int. Ed.* **2004**, *43*, 5639 – 5642; *Angew. Chem.* **2004**, *116*, 5757 – 5760; e) B. O. Okesola, A. Mata, *Chem. Soc. Rev.* **2018**, *47*, 3721 – 3736.

[3] a) H. Chen, W. Zhang, G. Zhu, J. Xie, X. Chen, *Nat. Rev. Mater.* **2017**, *2*, 17024; b) D. Sun, S. Zhou, W. Gao, *ACS Nano* **2020**, *14*, 12281 – 12290.

[4] a) R. van der Meel, E. Sulheim, Y. Shi, F. Kiessling, W. J. M. Mulder, T. Lammers, *Nat. Nanotechnol.* **2019**, *14*, 1007 – 1017; b) J. Shi, P. W. Kantoff, R. Wooster, O. C. Farokhzad, *Nat. Rev. Cancer* **2017**, *17*, 20 – 37.

[5] A. M. Vargason, A. C. Anselmo, S. Mitragotri, *Nat. Biomed. Eng.* **2021**, https://doi.org/10.1038/s41551-021-00698-w.

[6] a) D. Witzigmann, J. A. Kulkarni, J. Leung, S. Chen, P. R. Cullis, R. van der Meel, *Adv. Drug Delivery Rev.* **2020**, *159*, 344 – 363; b) E. Rideau, R. Dimova, P. Schwille, F. R. Wurm, K. Landfester, *Chem. Soc. Rev.* **2018**, *47*, 8572 – 8610.

[7] M. J. Mitchell, M. M. Billingsley, R. M. Haley, M. E. Wechsler, N. A. Peppas, R. Langer, *Nat. Rev. Drug Discovery* **2021**, *20*, 101 – 124.

[8] F. Zhang, G. Zhu, O. Jacobson, Y. Liu, K. Chen, G. Yu, Q. Ni, J. Fan, Z. Yang, F. Xu, X. Fu, Z. Wang, Y. Ma, G. Niu, X. Zhao, X. Chen, *ACS Nano* **2017**, *11*, 8838 – 8848.

[9] a) M. H. Y. Cheng, K. M. Harmatys, D. M. Charron, J. Chen, G. Zheng, *Angew. Chem. Int. Ed.* **2019**, *58*, 13394 – 13399; *Angew. Chem.* **2019**, *131*, 13528 – 13533; b) J. F. Lovell, C. S. Jin, E. Huynh, H. Jin, C. Kim, J. L. Rubinstein, W. C. W. Chan, W. Cao, L. V. Wang, G. Zheng, *Nat. Mater.* **2011**, *10*, 324 – 332.

[10] L. Zhu, Y. Guo, Q. Qian, D. Yan, Y. Li, X. Zhu, C. Zhang, *Angew. Chem. Int. Ed.* **2020**, *59*, 17944 – 17950; *Angew. Chem.* **2020**, *132*, 18100 – 18106.

[11] a) H. Su, J. M. Koo, H. Cui, *J. Controlled Release* **2015**, *219*, 383 – 395; b) Z. Zhou, J. Song, R. Tian, Z. Yang, G. Yu, L. Lin, G. Zhang, W. Fan, F. Zhang, G. Niu, L. Nie, X. Chen, *Angew. Chem. Int. Ed.* **2017**, *56*, 6492 – 6496; *Angew. Chem.* **2017**, *129*, 6592 – 6596; c) J. A. Kulkarni, D. Witzigmann, S. Chen, P. R. Cullis, R. van der Meel, *Acc. Chem. Res.* **2019**, *52*, 2435 – 2444; d) G. Arias-Alpizar, L. Kong, R. C. Vlieg, A. Rabe, P. Papadopoulou, M. S. Meijer, S. Bonnet, S. Vogel, J. van Noort, A. Kros, F. Campbell, *Nat. Commun.* **2020**, *11*, 3638; e) L. Tang, Z. Yang, Z. Zhou, Y. Ma, D. O. Kiesewetter, Z. Wang, W. Fan, S. Zhu, M. Zhang, R. Tian, L. Lang, G. Niu, X. Zhang, X. Chen, *Theranostics* **2019**, *9*, 1358 – 1368.

[12] Y. Shen, E. Jin, B. Zhang, C. J. Murphy, M. Sui, J. Zhao, J. Wang, J. Tang, M. Fan, E. Van Kirk, W. J. Murdoch, *J. Am. Chem. Soc.* **2010**, *132*, 4259 – 4265.

[13] X. Liang, C. Gao, L. Cui, S. Wang, J. Wang, Z. Dai, *Adv. Mater.* **2017**, *29*, 1703135.

[14] H. Su, W. Zhang, H. Wang, F. Wang, H. Cui, *J. Am. Chem. Soc.* **2019**, *141*, 11997 – 12004.

[15] J. H. Doroshow, R. M. Simon, *Cell* **2017**, *171*, 1476 – 1478.

[16] a) H. He, L. Liu, E. E. Morin, M. Liu, A. Schwendeman, *Acc. Chem. Res.* **2019**, *52*, 2445 – 2461; b) S. Hua, M. B. C. de Matos, J. M. Metselaar, G. Storm, *Front. Pharmacol.* **2018**, *9*, 790.

[17] G. P. Stathopoulos, J. Dimitroulis, D. Antoniou, C. Katis, D. Tsavdaridis, O. Armenaki, C. Marosis, P. Michalopoulou, T. Grigoratou, J. Stathopoulos, *Br. J. Cancer* **2005**, *93*, 1106 – 1111.

[18] S. Jiang, M. Xiao, W. Sun, D. Crespy, V. Mailänder, X. Peng, J. Fan, K. Landfester, *Angew. Chem. Int. Ed.* **2020**, *59*, 20008 – 20016; *Angew. Chem.* **2020**, *132*, 20183 – 20191.
[19] H. Wang, L.-P. Zhou, Y. Zheng, K. Wang, B. Song, X. Yan, L. Wojtas, X.-Q. Wang, X. Jiang, M. Wang, Q.-F. Sun, B. Xu, H.-B. Yang, A. C.-H. Sue, Y.-T. Chan, J. L. Sessler, Y. Jiao, P. J. Stang, X. Li, *Angew. Chem. Int. Ed.* **2021**, *60*, 1298 – 1305; *Angew. Chem.* **2021**, *133*, 1318 – 1325.
[20] A. M. Khalifa, M. A. Elsheikh, A. M. Khalifa, Y. S. R. Elnaggar, *J. Controlled Release* **2019**, *311 – 312*, 125 – 137.
[21] Y. Liu, G. Yang, T. Baby, Tengjisi, D. Chen, D. A. Weitz, C.-X. Zhao, *Angew. Chem. Int. Ed.* **2020**, *59*, 4720 – 4728; *Angew. Chem.* **2020**, *132*, 4750 – 4758.
[22] G. Hariri, A. D. Edwards, T. B. Merrill, J. M. Greenbaum, A. E. van der Ende, E. Harth, *Mol. Pharm.* **2014**, *11*, 265 – 275.

Manuscript received: June 29, 2021
Accepted manuscript online: July 18, 2021
Version of record online: August 11, 2021

